

# A tilted grating interferometer for full vector field differential x-ray phase contrast tomography

Simon Rutishauser,<sup>1,\*</sup> Tilman Donath,<sup>1,2</sup> Christian David,<sup>1</sup> Franz Pfeiffer,<sup>3</sup> Federica Marone,<sup>1</sup> Peter Modregger,<sup>1,4</sup> and Marco Stampanoni<sup>1,5</sup>

<sup>1</sup>Paul Scherrer Institut, 5232 Villigen PSI, Switzerland

<sup>2</sup>Dectris Ltd., 5400 Baden, Switzerland

<sup>3</sup>Department of Physics, Technische Universität München, 85747 Garching, Germany

<sup>4</sup>School of Biology and Medicine, University of Lausanne, 1015 Lausanne, Switzerland

<sup>5</sup>Institute for Biomedical Engineering, ETH Zürich, 8092 Zürich, Switzerland

\*[simon.rutishauser@psi.ch](mailto:simon.rutishauser@psi.ch)

**Abstract:** We report on a setup for differential x-ray phase-contrast imaging and tomography, that measures the full 2D phase-gradient information. The setup uses a simple one-dimensional x-ray grating interferometer, in which the grating structures of the interferometer are oriented at a tilt angle with respect to the sample rotation axis. In such a configuration, the differential phase images from opposing tomography projections can be combined to yield both components of the gradient vector. We show how the refractive index distribution as well as its  $x$ ,  $y$ , and  $z$  gradient components can be reconstructed directly from the recorded projection data. The method can equally well be applied at conventional x-ray tube sources, to analyzer based x-ray imaging or neutron imaging. It is demonstrated with measurements of an x-ray phantom and a rat brain using synchrotron radiation.

© 2011 Optical Society of America

**OCIS codes:** (110.7440) X-ray imaging; (340.7450) X-ray interferometry; (110.6955) Tomographic imaging; (110.3175) Interferometric imaging.

---

## References and links

1. R. Fitzgerald, "Phase-Sensitive X-Ray Imaging," *Phys. Today* **53**(7), 23–26 (2000).
2. A. Momose, "Recent Advances in X-ray Phase Imaging," *Jpn. J. Appl. Phys.* **44**, 6355–6367 (2005).
3. C. David, B. Nöhammer, H. Solak, and E. Ziegler, "Differential x-ray phase contrast imaging using a shearing interferometer," *Appl. Phys. Lett.* **81**, 3287–3289 (2002).
4. A. Momose, "Phase-sensitive imaging and phase tomography using X-ray interferometers," *Opt. Express* **11**, 2303–2314 (2003).
5. T. Weitkamp, A. Diaz, C. David, F. Pfeiffer, M. Stampanoni, P. Cloetens, and E. Ziegler, "X-ray phase imaging with a grating interferometer," *Opt. Express* **13**, 6296–6304 (2005).
6. F. Pfeiffer, T. Weitkamp, O. Bunk, and C. David, "Phase retrieval and differential phase-contrast imaging with low-brilliance X-ray sources," *Nat. Phys.* **2**, 258–261 (2006).
7. T. Donath, F. Pfeiffer, O. Bunk, W. Groot, M. Bednarzik, C. Grünzweig, E. Hempel, S. Popescu, M. Hoheisel, and C. David, "Phase-contrast imaging and tomography at 60 keV using a conventional x-ray tube source," *Rev. Sci. Instrum.* **80**, 053701 (2009).
8. T. Donath, F. Pfeiffer, O. Bunk, C. Grünzweig, E. Hempel, S. Popescu, P. Vock, and C. David, "Toward Clinical X-ray Phase-Contrast CT: Demonstration of Enhanced Soft-Tissue Contrast in Human Specimen," *Invest. Radiol.* **45**, 445–452 (2010).

9. F. Pfeiffer, C. Grünzweig, O. Bunk, G. Frei, E. Lehmann, and C. David, "Neutron Phase Imaging and Tomography," *Phys. Rev. Lett.* **96**, 215505 (2006).
10. C. Kottler, C. David, F. Pfeiffer, and O. Bunk, "A two-directional approach for grating based differential phase contrast imaging using hard x-rays," *Opt. Express* **15**, 1175–1181 (2007).
11. I. Zanette, T. Weitkamp, T. Donath, S. Rutishauser, and C. David, "Two-Dimensional X-Ray Grating Interferometer," *Phys. Rev. Lett.* **105**, 248102 (2010).
12. H. Wen, E. Bennett, R. Kopace, A. Stein, and V. Pai, "Single-shot x-ray differential phase-contrast and diffraction imaging using two-dimensional transmission gratings," *Opt. Lett.* **35**, 1932–1934 (2010).
13. H. Itoh, K. Nagai, G. Sato, K. Yamaguchi, T. Nakamura, T. Kondoh, C. Ouchi, T. Teshima, Y. Setomoto, and T. Den, "Two-dimensional grating-based X-ray phase-contrast imaging using Fourier transform phase retrieval," *Opt. Express* **19**, 3339–3346 (2011).
14. F. Pfeiffer, C. Kottler, O. Bunk, and C. David, "Hard X-Ray Phase Tomography with Low-Brilliance Sources," *Phys. Rev. Lett.* **98**, 108105 (2007).
15. M. Stampanoni, A. Groso, A. Isenegger, G. Mikuljan, Q. Chen, A. Bertrand, S. Henein, R. Betemps, U. Frommherz, P. Böhler, D. Meister, M. Lange, and R. Abela, "Trends in synchrotron-based tomographic imaging: the SLS experience," *Proc. SPIE*, **6318**, 63180M (2006).
16. C. David, J. Bruder, T. Rohbeck, C. Grünzweig, C. Kottler, A. Diaz, O. Bunk, and F. Pfeiffer, "Fabrication of diffraction gratings for hard X-ray phase contrast imaging," *Microelectron. Eng.* **84**, 1172–1177 (2007).
17. S. McDonald, F. Marone, C. Hintermüller, G. Mikuljan, C. David, F. Pfeiffer, and M. Stampanoni, "Advanced phase-contrast imaging using a grating interferometer," *J. Synchrotron Radiat.* **16**, 562–572 (2009).
18. R. Frankot and R. Chellapa, "A Method for Enforcing Integrability in Shape from Shading Algorithms," *IEEE Trans. Pattern Anal. Mach. Intel.* **10**, 439–451 (1988).
19. A. Agrawal, R. Raskar, and R. Chellapa, "What is the Range of Surface Reconstructions from a Gradient Field?" 9<sup>th</sup> European Conference on Computer Vision, **3951**, 578–591 (2006).
20. Z. Fu, A. Robles-Kelly, and F. Lu, "A Linear Programming Approach to Surface Fitting," 9<sup>th</sup> Biennial Conference of the Australian Pattern Recognition Society on Digital Image Computing Techniques and Applications, 189–195 (2007).
21. The out-of-plane component cancels out because the phase integration, which is implicit in the modified reconstruction kernel, is always performed along the same direction in the camera coordinate system. Considering for instance an integral from left to right through the PMMA cylinder at the bottom of Fig. 2(d), the signal at its left edge is  $\partial_x\Phi + \partial_z\Phi$  where the signal in the tomographic rotation plane is  $\partial_x\Phi > 0$  and the out-of-plane signal  $\partial_z\Phi < 0$ . Integrating through the same edge of the sample in Fig. 2(e), the out-of-plane signal has changed sign  $\partial_z\Phi > 0$ , while the in-plane signal has again the same sign as before  $\partial_x\Phi > 0$ . Reconstructing a slice using filtered back projection over a full sample rotation of  $2\pi$ , each projection pair corresponds to a single line in two-dimensional Fourier space. The out of plane component cancels out since it is once added and once subtracted to this line.
22. P. Zhu, J. Wang, Q. Yuan, W. Huang, H. Shu, B. Gao, T. Hu, and Z. Wu, "Computed tomography algorithm based on diffraction-enhanced imaging setup," *Appl. Phys. Lett.* **87**, 264101 (2005).

---

## 1. Introduction

Hard x-ray phase-contrast imaging in combination with tomographic reconstruction is a powerful tool for 3D investigations, especially of weakly absorbing biological specimens where it can provide better contrast than absorption tomography [1,2]. The grating interferometer based differential phase contrast (DPC) method has obtained increasing attention since its invention a few years ago [3–5], as it is compatible with conventional x-ray tube sources [6,7]. This opens up wide-spread applications, for instance in medical imaging [8]. Grating interferometry has also been applied to neutron phase contrast imaging and tomography [9].

The phase gradient is a two-dimensional vector, but the differential methods measure only one of its components, that is, only a directional derivative of the phase-shift projection  $\Phi$ . Knowledge of the two-dimensional gradient vector is crucial, because it enables tomographic reconstruction of the three-dimensional phase gradient vector field and more accurate recovery of  $\Phi$  and its tomographic reconstruction, reducing low-frequency reconstruction artifacts and phase clipping.

Two approaches to record the full gradient vector with a grating interferometer have been reported. One is to rotate the sample or the entire interferometer around the optical axis [10], though this requires an additional axis of rotation and is therefore hardly compatible with gantry

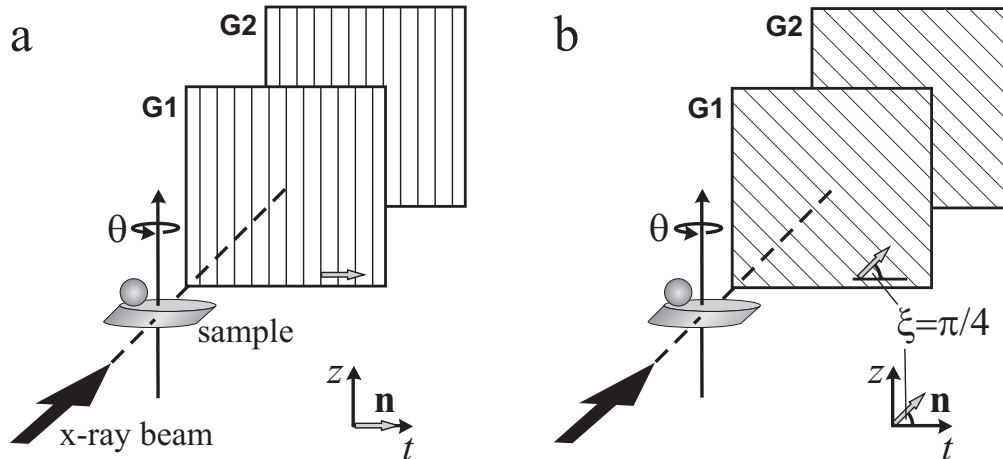


Fig. 1. Scheme of phase-contrast tomography using a one-dimensional grating interferometer. The sample is mounted on a rotation axis  $\theta$  to enable tomographic scans. Downstream of the sample are the beam splitter phase grating  $G_1$ , the absorbing analyzer grating  $G_2$  and an imaging detector (not shown here). (a) Conventional arrangement with the grating lines parallel to the sample rotation axis and (b) tilted grating interferometer arrangement with the grating structures tilted, here by an angle of  $\xi = \pi/4$ . The normal  $\mathbf{n}_\xi$  to the grating structures (gray arrows) points along the direction of the measured gradient component.

systems in medical tomography scanners. The other possibility is to use two-dimensional grating structures [11], which suffers from slow data acquisition as it requires phase stepping in two dimensions or, when used in single-shot mode, only provides reduced spatial resolution [12,13].

Here, we present a simple arrangement that allows to measure the full two-dimensional gradient vector using one-dimensional gratings with only a small modification to the conventional grating interferometry setup. Further, we show how projections acquired with this configuration can be used directly for tomographic reconstruction. Our arrangement avoids inconvenient rotation of interferometer or sample around the beam axis and is well suited for gantry systems in computed tomography (CT) scanners.

## 2. Grating interferometer and experimental setup

Figure 1(a) shows the conventional two-grating setup for DPC tomography at a synchrotron beamline. The sample rotation axis used for tomographic scans is vertical, allowing for immersion of the sample in a liquid environment. Using vertical grating structures, oriented parallel to the sample rotation axis, the phase gradient component in the plane of rotation is recorded by phase stepping, i.e. translating one of the gratings in several steps over at least one grating period. This setup enables direct tomographic reconstruction of the refractive index decrement [14].

In the tilted-grating setup shown in Fig. 1(b) the grating structures are tilted by an angle  $\xi$  with respect to the sample rotation axis. The grating structures are no longer parallel to the sample rotation axis. This enables measurements of the out-of-plane gradient component  $\partial_\xi \Phi$  along a normal to the grating structures  $\mathbf{n}_\xi = (\cos \xi, \sin \xi)$ , indicated in Fig. 1 by gray arrows.

The full 2D gradient  $\nabla_{tz} \Phi(t, z, \theta)$  can be determined from the measurement of two opposing projection images  $g_\theta$  and  $g_{\theta+\pi}$  recorded at tomographic projection angles  $\theta$  and  $\theta + \pi$ , respectively. Although the directional derivatives in both projections are measured along the same direction  $\mathbf{n}_\xi$  in the fixed detector coordinate system  $tz$ , they point into two linearly independent directions in the sample system (which is rotating around  $z$ ).

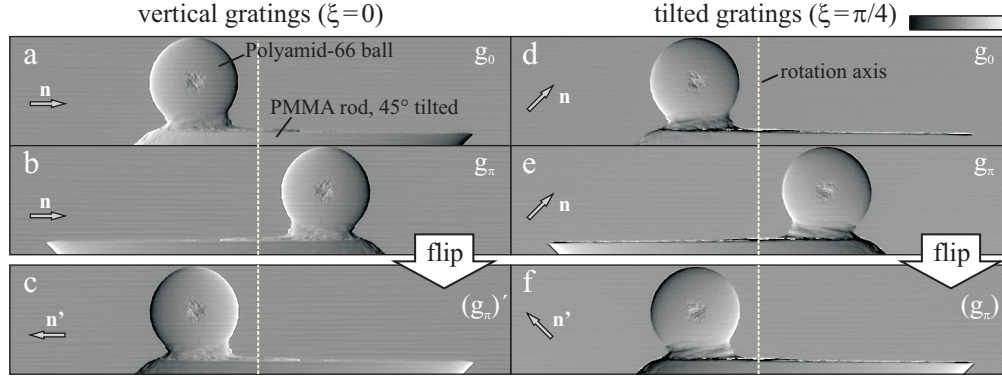


Fig. 2. Projections of the x-ray phantom. (a,b) DPC projection pair  $g_0$  and  $g_\pi$  recorded with vertical gratings at tomographic projection angles  $\theta = 0$  and  $\pi$  respectively. (c) flipped projection  $(g_\pi)'$ , same data as (b) but flipped at the sample rotation axis. (d,e) DPC projection pair recorded with tilted gratings at  $\xi = \pi/4$  ( $45^\circ$ ). (f) projection data from (e) flipped at the sample rotation axis. While (a) and (c) only provide the horizontal component of the phase gradient, the projections recorded with tilted gratings (d) and (f) yield two linearly independent components and thus the full 2D gradient vector. All images are displayed with a linear gray scale with deflection angles in the range of  $[-2.6, 2.6]$   $\mu\text{rad}$ .

To demonstrate this, we imaged an x-ray phantom as schematically shown in Fig. 1 with vertical grating lines and with the gratings tilted to  $\xi = \pi/4$  ( $45^\circ$ ).

All measurements were carried out at the Tomcat beamline (X02DA, described in Ref. [15]) of the Swiss Light Source (SLS) at a photon energy of 25 keV ( $\Delta E/E \approx 2\%$ ) selected with a [W/Si]<sub>100</sub> multilayer monochromator. The source-to-G1 distance was 25 m and the distance between G1 and G2 was 0.12 m, corresponding to the third fractional Talbot distance of the phase grating. The phase grating G1 ( $\pi$  shifting, period  $p_1 = 3.98 \mu\text{m}$ ) and the absorption grating G2 ( $p_2 = 2.00 \mu\text{m}$ ) were made of silicon and silicon filled with electroplated gold respectively [16]. The x-ray camera consisted of a luminescent screen ( $100 \mu\text{m}$  YAG:Ce) lens-coupled (1:1 magnification, f-number 2.5, 150 mm focal length) to a CCD camera (PCO2000). The exposure time was 125 ms per image. We selected a  $1529 \times 413$  pixel region of interest, with an effective pixel size of  $7.4 \mu\text{m}$ , which is the factor limiting the spatial resolution of the imaging system. The grating interferometer at the Tomcat beamline is described in more detail elsewhere [17].

At each projection angle a phase-stepping scan was recorded by translating the grating G2 in 10 equidistant steps over two grating periods. All recorded phase-stepping images were dark- and flat-field corrected and processed to obtain projections of the differential phase signal [5].

### 3. Phase gradient vector in projections

Differential phase contrast projection images of the x-ray phantom for the setup with vertical and with tilted gratings are shown in Fig. 2. For each setup, the figure shows the projections  $g_0$  and  $g_\pi$  recorded at projection angles  $\theta = 0$  and  $\pi$  respectively.

The DPC images  $g_0$  and  $g_\pi$  are mirror images of each other, flipped at the sample rotation axis ( $z$  axis), i.e. with reversed  $t$  direction and inverted sign of the gradient component along  $t$  [Fig. 2(d,e)]. To overlay the measured directional derivatives, we have to flip the  $t$ -direction of image  $g_\pi$  to obtain the flipped image  $(g_\pi)'$  as shown in Fig. 2(f). Flipping the gradient projection also changes the direction of the measured gradient, which becomes

$$\mathbf{n}_{\xi'} = \begin{pmatrix} \cos \xi' \\ \sin \xi' \end{pmatrix} = \begin{pmatrix} -\cos \xi \\ \sin \xi \end{pmatrix} = \mathbf{n}_{\pi-\xi}. \quad (1)$$

Thus, the directional derivative in the flipped image  $(g_\pi)'$  [Fig. 2(f)] is measured along  $\mathbf{n}_{\xi'}$  with the angle  $\xi' = \pi - \xi = \frac{3}{4}\pi$  ( $135^\circ$ ), perpendicular to the measurement  $g_0$  along  $\mathbf{n}_\xi$  with  $\xi = \frac{\pi}{4}$  [ $45^\circ$ , Fig. 2(d)].

The gradient vector in the  $tz$  coordinate system is easily obtained from the gradient images  $g_0$  and  $(g_\pi)'$ , which are measurements of  $\partial_\xi\Phi$  and  $\partial_{\pi-\xi}\Phi$  respectively, by a coordinate transform

$$\partial_t\Phi = \frac{g_0 - (g_\pi)'}{2\cos\xi} \quad \text{and} \quad \partial_z\Phi = \frac{g_0 + (g_\pi)'}{2\sin\xi}. \quad (2)$$

The factors  $1/\cos\xi$  and  $1/\sin\xi$  account for the tilt angle dependency of the sensitivity. As the grating tilt angle  $\xi$  approaches  $\frac{\pi}{2}$ , the sensitivity and hence the measurement quality along  $z$  increase. In the special case of a conventional setup with vertical gratings ( $\xi = 0$ ) for instance, we measure the directional derivatives  $g_0 = \partial_0\Phi = \partial_t\Phi$  [Fig. 2(a)] and  $(g_\pi)' = (\partial_\pi\Phi)' = -\partial_t\Phi$  [Fig. 2(c)]. These differ only by sign and do not provide complementary information. The ideal tilt angle depends on the experimental conditions, using  $\xi = \frac{\pi}{4}$  and thus equal sensitivity along both  $t$  and  $z$  is a good starting point.

From the two-dimensional projection gradient  $\partial_t\Phi$  and  $\partial_z\Phi$ , integrated phase projections can be obtained by means of existing algorithms [10, 18–20]. The integrated phase projections can then be used for tomographic reconstruction of the refractive index decrement  $\delta$ .

#### 4. Tomographic reconstruction

In the setup with vertical gratings, tomographic reconstruction of the refractive index decrement  $\delta$  from the recorded differential phase projections  $g_\theta$  is performed using filtered back projection with a modified frequency-filter kernel  $\tilde{h}(v') = (1/2\pi i)\text{sgn}(v')$  with  $\text{sgn}(v')$  the sign function [14]. This reconstruction can be carried out for data from the tilted grating setup as well. No modification is required, other than multiplication by a constant factor of  $1/\cos\xi$  accounting for the modified sensitivity, which is the same factor as in the coordinate transform used to obtain the gradient component along  $t$  [Eq. (2)]. The out-of-plane gradient components of each of the mirror projection pairs cancel out, when reconstructing data recorded over  $2\pi$  sample rotation [21].

From the data recorded with the tilted grating setup, the gradient in  $z$  direction can be reconstructed directly as well. This is achieved by using the conventional filtered back projection kernel  $\tilde{k}(v') = |v'|$ . In this case, the gradient components in the rotation plane cancel out.

With a tilted grating interferometer, the complete three-dimensional phase gradient vector field can be reconstructed. The reconstruction of the in-plane gradient components  $\partial_x\delta$  and  $\partial_y\delta$  is described elsewhere [22]. This opens up another way to obtain the refractive index decrement reconstruction, based on integrating its reconstructed three-dimensional gradient vector field.

To demonstrate the tilted grating setup in tomography, scans of the phantom shown in Fig. 2 and a biological sample - a rat brain embedded in paraffin were recorded. The tomographic scans were performed by rotating the sample over  $360^\circ$  in 720 (phantom, with  $2 \times 2$  pixel binning) and 1440 (rat brain) equiangular steps.

Figure 3(a) shows a reconstructed slice through the homogeneous PMMA cylinder at the bottom of the projections in Fig. 2, while Fig. 3(d) shows a slice through the rat brain. The difference between two neighboring slices  $\Delta_z\delta$ , as an approximation of the gradient in  $z$  direction is shown in Fig. 3(b,e). The difference image  $\Delta_z\delta$  of the phantom suffers from reconstruction artifacts, such as dark rings as well as line artifacts due to phase clipping at the boundaries. The latter are due to the large phase gradient between the sample and the surrounding air. Low-frequency inhomogeneities within the sample and background are observed for both phantom and rat brain. These occur due to vibrations of the monochromator and drift in the setup and

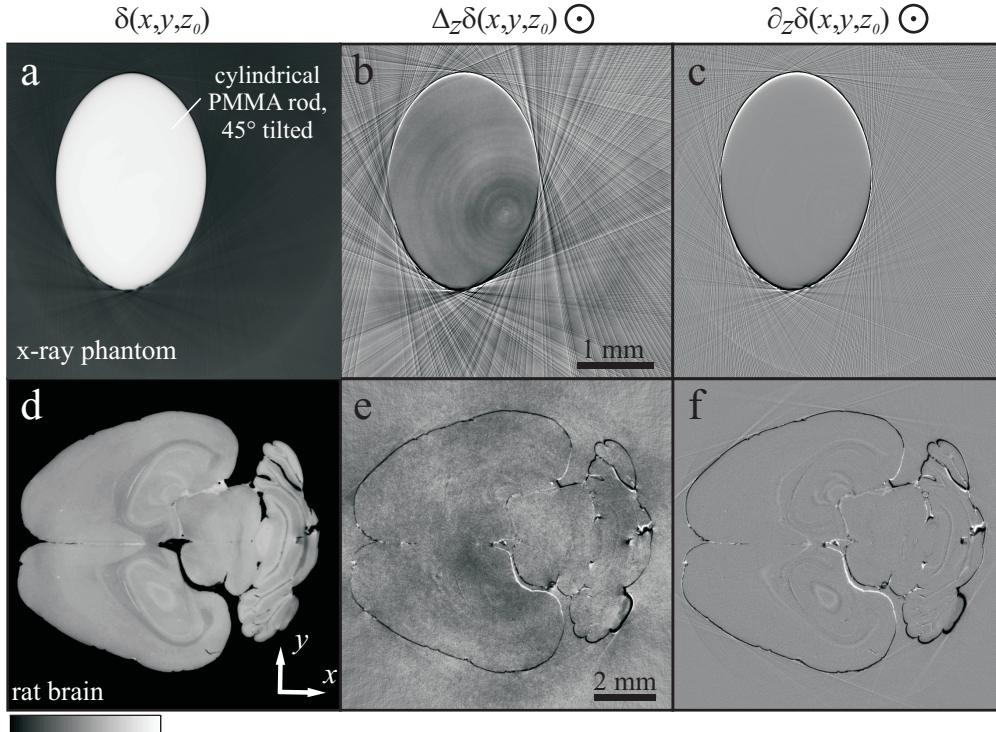


Fig. 3. Tomographic phase reconstructions of x-ray phantom (top) and rat brain (bottom). The phantom reconstruction shows a slice through the homogeneous PMMA rod. (a) and (d) show the refractive index decrement  $\delta$ , averaged from two neighboring slices. (b) and (e) show the  $z$  gradient calculated from the difference of the two neighboring slices. (c) and (f) show the direct reconstruction of the  $z$  gradient, which uses the additional information gained by tilting the gratings. All images are displayed with a linear gray scale with the following ranges: (a)  $\delta = [-0.1, 0.4] \cdot 10^{-7}$ , (b,c)  $\Delta_z \delta = \partial_z \delta = [-1.8, 1.8] \cdot 10^{-3} \text{ m}^{-1}$ , (d)  $\delta = [3, 4] \cdot 10^{-7}$  and (e,f)  $\Delta_z \delta = \partial_z \delta = [-1.5, 1.5] \cdot 10^{-3} \text{ m}^{-1}$ .

are amplified by the comparatively high weight given to low-frequency components by the reconstruction filter kernel  $\tilde{h}(v')$ .

The gradient in  $z$  direction as reconstructed directly from the tilted grating data is shown in Fig. 3(c,f). This reconstruction  $\partial_z \delta$  is much cleaner and does not show the low-frequency artifacts observed in the finite difference images. The line artifacts in Fig. 3(c) are also reduced.

Figure 4 shows sagittal slices of the rat brain. All components of the gradient have been reconstructed [Fig. 4(a-c)]. The reconstruction of  $\delta(x, y, z)$  based on the in-plane gradient data, as available in the conventional setup with vertical gratings shows strong horizontal stripe artifacts [Fig. 4(d)]. A much cleaner reconstruction [Fig. 4(e)] can be obtained by using a suitable phase integration algorithm as described i.e. in Ref. [20] to combine the reconstructed gradient  $\partial \delta_x$  [Fig. 4(a)] with the gradient  $\partial \delta_z$  [Fig. 4(c)], which becomes available in the tilted grating setup.

## 5. Conclusion

In conclusion, the presented grating-interferometer arrangement with tilted gratings allows the phase gradient vector to be recorded in a simple manner from a pair of mirror projections. It requires rotation of the object around an axis perpendicular to the optical axis only, which is readily available in tomography setups. Hence, obtaining a second linearly independent gradient direction is easy, in comparison to existing techniques, which perform a complicated rotation of

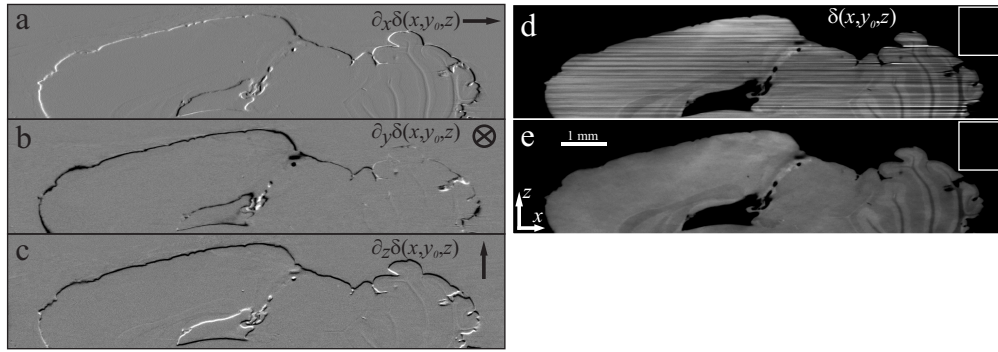


Fig. 4. Tomographic phase reconstruction of sagittal slices of a rat brain. On the left side are the three components of the reconstructed gradient (a)  $\partial_x \delta$  in horizontal direction, (b)  $\partial_y \delta$  perpendicular to the sagittal plane and (c)  $\partial_z \delta$  in vertical direction. (d) shows the reconstruction of  $\delta$  using only the gradient components in the tomographic rotation plane, as available in a conventional interferometer setup with vertical gratings. The standard deviation within the white square of constant  $\delta$  is  $\sigma_\delta = 3.9 \cdot 10^{-9}$ . (e) shows the much cleaner reconstruction of  $\delta$  obtained by combining the reconstructed gradient components  $\partial_x \delta$  and  $\partial_z \delta$ . Here the standard deviation is  $\sigma_\delta = 1.6 \cdot 10^{-9}$ . All images are displayed with a linear gray scale with the following ranges: (a-c)  $\partial \delta = [-1.5, 1.5] \cdot 10^{-3} \text{ m}^{-1}$  and (d,e)  $\delta = [3, 4] \cdot 10^{-7}$ .

interferometer or sample around the beam axis, or use more complex two-dimensional grating interferometers. The obtained additional gradient information can be used for reconstructing the three-dimensional phase gradient field and for improving phase integration and reconstruction. The arrangement is not limited to grating-based imaging and should also be applicable for all other one-dimensional differential phase-contrast techniques including diffraction-enhanced and analyzer-based x-ray imaging.

### Acknowledgements

The authors would like to thank E. Hempel, S. Popescu, and M. Hoheisel (Siemens AG) for fruitful discussions, C. Grünzweig and J. Bruder for grating fabrication and G. Mikuljan (Paul Scherrer Institut) for his assistance in preparing the x-ray phantom. F.P. acknowledges support through the DFG Cluster of Excellence "Munich-Centre for Advanced Photonics" and the European Research Council (FP7, Starting grant #240142). P.M. acknowledges support through the Centre d'Imagerie Biomédicale (CIBM) of the UNIL, UNIGE, HUG, CHUV, EPFL and the Leenaards and Jeantet Foundations.